IEEE VTS Motor Vehicles Challenge 2023: A Multi-physical Benchmark Problem for Next Generation Energy Management Algorithms

Jonathan Brembeck
Institute of System Dynamics and Control (SR)
German Aerospace Center (DLR)
Oberpfaffenhofen, Germany
jonathan.brembeck@dlr.de
ORCID: 0000-0002-7671-5251

Ricardo Pinto de Castro
Department of Mechanical Engineering
University of California Merced
rpintodecastro@ucmerced.edu
ORCID: 0000-0002-5546-3999

Jakub Tobolář
Institute of System Dynamics and Control (SR)
German Aerospace Center (DLR)
Oberpfaffenhofen, Germany
jakub.tobolar@dlr.de
ORCID: 0000-0002-4888-4664

***Abstract*—This article presents a benchmark problem that researchers can use to evaluate the performance of energy management algorithms for multi-energy source and multi-motor electric vehicles. The model makes use of Modelica, an open source, a-causal, object-oriented language for modeling cyber-physical systems in multi-domains (e.g. electrical, mechanical, thermal) of the vehicle components. The model also includes the aspect of three-dimensional mechanics, which enables completely new degrees of freedom in the controller design in comparison to one-dimensional approaches. To support interoperability among multiple design tools, the Modelica vehicle model is provided as a Functional Mockup Unit, an industry standard for exchange of simulation models. A set of standardized input-output interfaces and key performance metrics is also provided in the benchmarking problem, enabling the systematic ranking of multiple energy management strategies.**

Keywords—energy management, vehicle dynamics control, electro-mobility, trajectory control, energy management, battery model, , Modelica, Functional Mockup Interface, hydrogen fuel cell, multi-physical modelling, drivetrain models

I. INTRODUCTION

In order to stimulate advances in vehicular energy and power management, the IEEE Vehicular Technology Society (VTS) initiated the VTS Motor Vehicles Challenge in 2016. The competition's themes have focused on energy management of hybrid energy storage systems (fuel cells/batteries/supercapacitors [1] [2] [3] [4]) and their applications to cars ([5] [6]), trucks [7] and trains [8]. These competitions provide benchmark problems where researchers can evaluate and compare the performance of their energy management algorithms against other research groups.

In this year's competition we bring a new dimension to the challenge: torque allocation in multi-motor electric vehicles. In addition to managing a hybrid energy storage system, the competitors are asked to develop torque allocation for a four-wheeled vehicle with three traction motors: two (rear) in-wheel motors and one front motor. This multi-motor configuration offers various advantages. It can enhance energy efficiency of the vehicle by enabling energy recuperation in both front and rear axle [9] and also decreasing tire slip losses [10]. It improves motion control of the vehicle by extending the maximum lateral acceleration [11] and decrease response of inner (yaw-rate) control loops. This last feature is particularly attractive to improve tracking performance and vehicle dynamics stability of path/trajectory following algorithms of autonomous vehicles [12]. It also offers redundant traction actuators that can be exploited by fault tolerant controllers to improve vehicle reliability [13].

As reference vehicle for this year's competition we employed an adapted version of the DLR ROboMObil ([14] [15] [16]), which is extended here with a hydrogen fuel cell. To model this vehicle, we make use of Modelica [15], an open source, a-causal, object-oriented language that allows the modeling of cyber-physical systems in multi-domains, e.g electrical, thermal or mechanical. It also offers powerful model inversion capabilities, which facilitate the design of non-linear motion control algorithms [16].

Since there is a manifold of simulators on the market, we decided to export the vehicle model through the functional mockup interface (FMI) [15] technology. This allows the competitors to develop a control strategy using their tool of choice or even make it part of a machine learning process. Our simulation model gives the benefit of a very high computational efficiency, with an average real-time factor larger than twenty on a standard PC, which can be particularly useful to accelerate the development of learning-based control algorithms (e.g. [19]).

The paper is arranged as follows: chapter II gives a general overview of the challenge; chapter III introduces the Modelica model of the ROboMObil; Chapter IV describes the evaluation process and ranking of energy management algorithms. Chapter V summarizes all development steps and provides a look into future research.

II. OVERVIEW OF THE CHALLENGE

As depicted in Figure 1, the challenge considers the ROboMObil vehicle with a hybrid energy storage system (fuel cell & hydrogen tank and battery), two in-wheel electric motors installed in the rear axle (τ_{RL}, τ_{RR}), one central front

motor (τ_{FM}), and a front steer-by-wire actuation (δ). These actuators are manipulated by the vehicle's motion controller in order to track a pre-defined reference velocity (v^*) and track curvature (ρ^*).

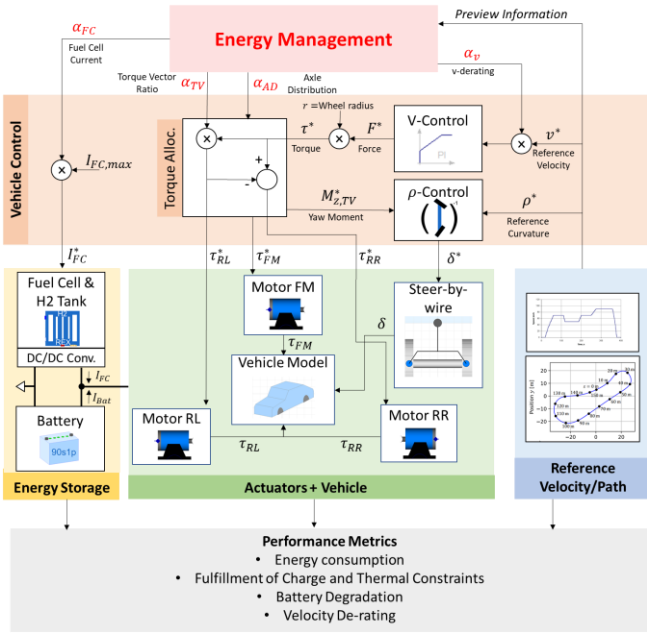

Figure 1: Block diagram of the benchmark problem. Note: the competitors are invited to develop the top red block, the energy management algorithm.

The competitors are invited to develop the energy management algorithm (EMA) for the vehicle. The EMA determines the operating conditions for the two energy storage devices and the three electric motors; minimization of the energy consumption and battery degradation are some of the main goals of the EMA.

A. *Energy Storage and Vehicle Actuators*

The hybrid energy storage is composed of a 20kW fuel cell and 20 kWh Li-ion battery. A DC/DC converter is connected to the fuel cell in order to regulate its current (I_{FC}) and power flow between the hybrid storage elements. The hybridization with a hydrogen range extender (REX), being composed of the fuel cell and a hydrogen tank, enables the reduction of usage of rare elements like Lithium while enhancing the vehicle's range. Both the fuel cell & H2 tank and the battery provide energy to the two in-wheel motors and the central front motor. Because of their decoupled architecture, the in-wheel motors can generate non-symmetric torques in the left and right rear wheels and, thus induce additional yaw-moment to the vehicle's chassis. This yaw-moment can be exploited to enhance vehicle handling and safety [20]; it can also decrease the amount of front steering, thus reducing tire slip losses [10]. Additionally, a steer-by-wire actuator is installed in the front axle to modify the steering angle δ.

B. *Mission Planning and Vehicle Control*

We assume that the planning of the vehicle's mission is defined in advance, e.g. using trajectory planning methods such as [21]. The mission is characterized by a reference vehicle velocity $v^*(t)$ and the track curvature $\rho^*(t)$ over a given time horizon $t \in [0, t_{end}]$.

The motion controller tracks v^* through manipulation of the reference traction force F^*. This reference force is converted into a reference torque $\tau^* = F^* r$, with r being the wheel radius, which is then divided between the front and rear axle

$$\tau_F^* = \tau^* \alpha_{AD}, \qquad \tau_R^* = \tau^* (1 - \alpha_{AD}), \tag{1}$$

where α_{AD} indicates the variable front/rear axle distribution. Afterwards, the rear axle torque is allocated into left and right motor torques using a normalized torque vector ratio $\alpha_{TV} \in [0, 1]$:

$$\tau_{RR}^* = \tau_R^* \alpha_{TV}, \qquad \tau_{RL}^* = \tau_R^* (1 - \alpha_{TV}). \tag{2}$$

When $\alpha_{TV} = 0.5$, both motors receive the same torque; $\alpha_{TV} = 1$ allocates all the torque solely to the right motor and $\alpha_{TV} = 0$ solely to the left motor. The reference curvature ρ^* is tracked through the manipulation of the steering angle δ^*, while considering the additional yaw-moment generated by the torque vectoring. Note that, throughout this document, the superscript x^* is used to denote the desired value for the variable x.

C. *Energy Management Algorithm (EMA)*

The EMA is responsible for computing four control variables, cf. the red variables in Figure 1 top:

1. the normalized fuel cell current, $\alpha_{FC} \in [0,1]$, which affects the power split between the battery and the fuel cell.
2. the axle torque distribution ratio, $\alpha_{AD} \in [0,1]$, to determine the front and rear distribution of the desired torque τ^*, see eq. (1).
3. the torque vectoring ratio, $\alpha_{TV} \in [0,1]$, to determine the torque allocation between right and left motors, see eq. (2).
4. the velocity derating factor, $\alpha_v \in [0,1]$, which decreases the reference velocity to $\alpha_v v^*$ (see Figure 1); it offers an additional degree of freedom to prevent violation of safety constraints in the system (e.g. over-discharge of the battery).

The EMA provided by the competitors will be evaluated using a wide range of performance metrics, including energy consumption, violation of safety constraints, battery degradation and fulfillment of the vehicle's mission (also referred as velocity derating in the sequel). These metrics will be defined in more detail in Section IV.

The EMA will have access to several states of the vehicle and energy storage, such as battery state of charge, temperature, etc. Additionally, it will also receive a short preview of future values of the velocity and curvature references:

$$\hat{v}(t + \Delta t), \hat{\rho}(t + \Delta t), \tag{3}$$

where $\Delta t \in [0, \Delta t_{max}]$ and Δt_{max} is the preview window which is available in map data systems with a virtual horizon. This preview information can be generated by the trajectory planning module of the vehicle.

III. Components Modeling

In this section we briefly describe the Modelica model of the ROboMObil [16] vehicle model as depicted in Figure 1. The aim is to describe the most relevant physical laws and

effects with the focus on a fast and reliable simulation, which is necessary for a fast assessment of the EMAs or a machine learning process to synthesis the controller.

A. The Chassis Model

To capture the fundamental dynamics of the RObоMObil, we use a double track model embedded in a planar mechanics [22] with three degrees of freedom: the vehicle can move in longitudinal and lateral direction and rotate about the vertical axis. The chassis model, depicted in Figure 2, consists of a front and rear axle, car body and air resistance.

In addition, the model contains three types of interfaces: mechanical (gray circles), thermal (red squares) and control (yellow connectors). The mechanical interfaces are used to exchange position and torque/force of mechanical elements. The heat interface captures the heat flow between components, and allows to quantify the energy losses that are eventually dissipated to the environment. The control interfaces contain auxiliary signals that are generated by sensors (e.g. acceleration signal produced by inertial measurement unit) and control modules (e.g., steering actuator demand). The rigid front axle is assembled from an open differential that distributes the torque of the central front motor to the left and right wheel with slip-based tire models, as well as a steering mechanism that equally transmits the steering input onto both left and right front wheels. The rigid rear axle is composed of two slip-based tire models.

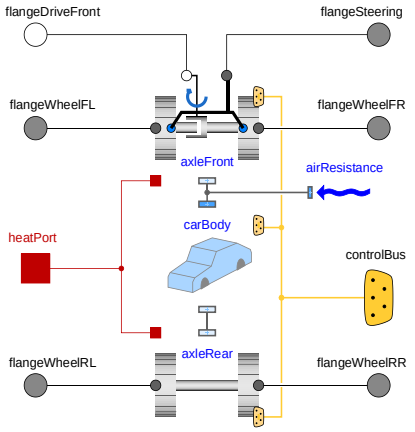

Figure 2: Structure of the Modelica planar vehicle model

B. Slip-based Tire Model with Losses

RObоMObil's four wheels are modelled with a slip-based tire model [22] which is extended with loss effects. To simplify the model, tire load fluctuation during cornering or braking/accelerating are neglected and the wheel is bounded to the track-plane (holonomic-constraint). While operating at constant load f_N, the slip velocity v_{slip} at the contact patch determines the slip forces according to Coulombs's law for dry-friction characteristics,

$$f_i = -f_N \, \mu(v_{\text{slip}}) \, \frac{v_{\text{slip},i}}{v_{\text{slip}}}. \qquad (4)$$

eq. (4) can be used for both the longitudinal ($i = long$) and the lateral ($i = lat$) velocity, resolved in the wheel coordinate system. The friction coefficient μ depends on the slip velocity v_{slip}, which is in [22] constructed by two pairs of parameters (v_{adhesion}, μ_A) and (v_{slide}, μ_S). The former pair determines maximum friction μ_A at $v_{\text{slip}} = v_{\text{adhesion}}$. The latter pair specifies a sliding area of friction μ_S at slip velocities $v_{\text{slip}} \geq v_{\text{slide}}$.

The rolling motion of the wheel can be actuated by the driving or braking torque input (cf. flangeWheel** - Figure 2). The tire losses comprise losses at tire/road contact area due to the dry-friction contact.

C. Battery Model with Aging Degradation

To obtain a good tradeoff between simulation speed and modeling accuracy, we modeled the battery with an equivalent electrical circuit model. This circuit consists of an ideal voltage source (U_{OCV}) in series with an internal resistance (R_i). The terminal voltage of the cell is described as

$$u_{\text{cell}} = U_{OCV}(SoC_b) - R_i(SoC_b) \cdot i_{\text{cell}}, \qquad (5)$$

where i_{cell} is the current in the battery cell.

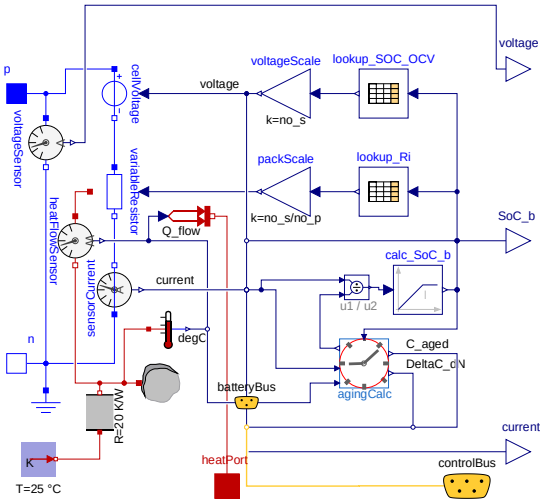

Figure 3: The equivalent circuit battery model in Modelica

Both the internal voltage and resistance depend on the battery state of charge (SoC_b), a normalized indicator for the amount of charge stored in the battery. Lookup tables are employed to characterize this variation, but are limited to room temperature values. A more complex implementation with temperature dependency is given in [22].

In Figure 3 the functional model of the battery pack is shown. On the left side we have the electrical connectors (in blue), which propagate the electric signals (voltage and current) to the other components in the vehicle, while on the right side we have the SoC_b calculation realized by an integrator ($calc\_SoC_b$), in dependency of the nominal cell capacity $C_{cell,0}$. The pack is scaled by the number of in serial no_s and in parallel no_p connected cells. The battery model also contains a simple thermal model that captures heat flow between the battery cell and a (constant-temperature) environment using a thermal resistor.

The battery model also includes an aging model (*agingCalc* in Figure 3) for predicting the capacity degradation of the battery due to the charge/discharge events. This aging is

computed using the average current (i_{avg}) and temperature (T_{avg}) of the battery over a discharge cycle, as described in [24]. The normalized cell capacity loss during the drive cycle ΔC_{cell} is calculated as

$$\begin{aligned}\Delta C_{\text{cell}}(i_{avg}, T_{avg}, N) &= \\ &= \underbrace{\theta_1 \exp\left(-\frac{\theta_4}{T_{avg}} + \left(\theta_2 + \frac{\theta_5}{T_{avg}} i_{avg}\right)\right)}_{\text{start of battery lifetime – slow aging}} \\ &+ \underbrace{\theta_8 \exp(N - N_{\text{knee}}\theta_7)}_{\text{"late" battery lifetime – fast aging}}\end{aligned} \tag{6}$$

where θ_i are aging parameters taken from experiments carried out in [24]. The parameter N is the number of discharge cycles and N_{knee} is a parameter point where the battery aging accelerates. The remaining cell capacity, in dependency of the initial cell capacity $C_{\text{cell},0}$ is defined as

$$C_{\text{aged}} = (1 - \Delta C_{\text{cell}}) C_{\text{cell},0} \tag{7}$$

To facilitate the evaluation of the EMA, we focus on the rate of aging of the battery during the driving cycle. It is determined via a linearization of ΔC_{cell} around the current number of cycles $\bar{N}$ as follows

$$\begin{aligned}\frac{\mathrm{d}\Delta C_{\text{cell}}(i_{avg}, T_{avg})}{dN} &= \left.\frac{\mathrm{d}\Delta C_{\text{cell}}(i_{avg}, T_{avg}, N)}{\mathrm{dN}}\right|_{N=\bar{N}} \\ &= \theta_1 \exp\left(-\frac{\theta_4}{T_{avg}} + \left(\theta_2 + \frac{\theta_5}{T_{avg}} i_{avg}\right)\right) \theta_3 \bar{N}^{\theta_3 - 1}\end{aligned} \tag{8}$$

D. Quasi-Stationary Electric Motor Model

The three traction motors installed in the vehicle (cf. Figure 1) rely on permanent magnet synchronous machines (PMSM). They are represented using a quasi-stationary model (Figure 4) with the variables listed in Table 1. The fundamental electric machine equations $d\Psi_d/dt$ and $\mathrm{d}\Psi_\mathrm{q}/\mathrm{d}t$ of the stator flux are given as:

$$\frac{d\Psi_d}{dt} = U_d - R_s I_d + \Omega_L \underbrace{L_1 I_\mathrm{q}}_{\Psi_\mathrm{q}} \tag{9}$$

$$\frac{\mathrm{d}\Psi_\mathrm{q}}{\mathrm{d}t} = U_q - R_\mathrm{s} I_\mathrm{q} - \Omega_\mathrm{L} \underbrace{(\Psi_\mathrm{PM} + L_1 \cdot I_\mathrm{d})}_{\Psi_\mathrm{d}} \tag{10}$$

These equations are easily implemented in Modelica using the acausal equation environment, i.e. all equation hold for the four quadrants of operation of the electric machine and are not dependent on any signal flow direction.

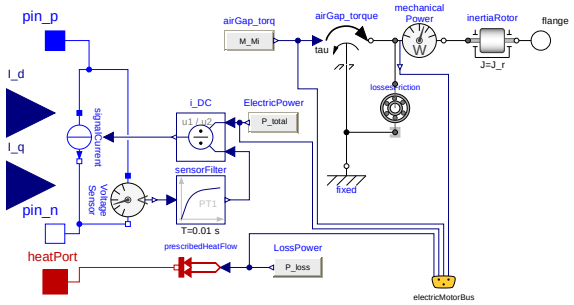

Figure 4: Quasi-stationary PMSM model

To prevent a slow simulation, the electric motor model and its controller are designed in the rotating d/q-frame and the reverse transformation to the a/b/c phases is not explicitly implemented. The closed-loop response of the motor current (I_q) controller is approximated by a second-order transfer function with cut-off frequency 100Hz.

Table 1: PMSM variables description

Quantity	Unit	Description
$U_{\mathrm{d}/q}$	V	Voltage in d-/q-axis
$I_{d/q}$	I	Current in d-/q-axis
L_1	H	Inductance in d- & q-axis
R_s	Ω	Warm resistance per phase
p	-	Pole pair number
ψ_{PM}	Wb	Magnetic flux of permanent magnets
$\psi_{d/q}$	Wb	d-/q- component of stator flux
ω_L	rad/s	(Normed) Electrical angular velocity of rotor

The model of the electric machine neglects reluctance influences ($L_\mathrm{d} = L_\mathrm{q} = L_1$). Its air-gap torque is calculated as follows:

$$\tau_{jk} = M_{\text{Mi}} = 3/2 \cdot p \cdot \Psi_{\text{PM}} \cdot I_\mathrm{q}. \tag{11}$$

Besides this quasi-stationary electric machine model, we also consider the following energy losses within the PMSM, summed up in $P_{loss} = \sum(\text{eqs.}\,(12) - (15))$ in Figure 4:

Inverter losses (switching and basic load)

$$P_{\text{loss,inv}} = P_{\text{inv,const}} + k_{\text{inv}} \cdot I_q. \tag{12}$$

Copper losses (coil resistance)

$$P_{\text{cop}} = \left(\sqrt{3/2} \cdot I_\mathrm{q}\right)^2 \cdot R_\mathrm{s}. \tag{13}$$

Iron losses (also known as core losses)

$$P_{\text{iron}} = k_{\text{hyst}} \cdot \omega_m + k_{\text{eddy}} \cdot \omega_m^2. \tag{14}$$

Mechanical losses (friction effects e.g. bearings)

$$P_{\text{fric}} = k_{\text{fric}} \cdot \omega_m. \tag{15}$$

E. The Hydrogen Fuel Cell Model

The fuel cell model relies on a quasi-stationary model as proposed in [25] and depicted in Figure 5.

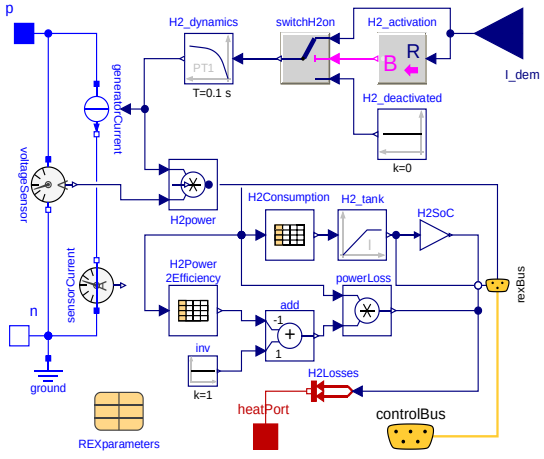

Figure 5: Functional hydrogen range extender model

Whenever a demanded current I_{dem} exceeds a minimum threshold ($1A$ in our model), the functional model approximates the fuel cell's output current using first order system dynamics. The fuel consumption relies on two tables. The first table maps the necessary hydrogen mass flow that is taken from the tank (Figure 6 – blue line), modelled as an integrator, whereas the second table maps the efficiency (Figure 6 – green line) depending on the point of operation.

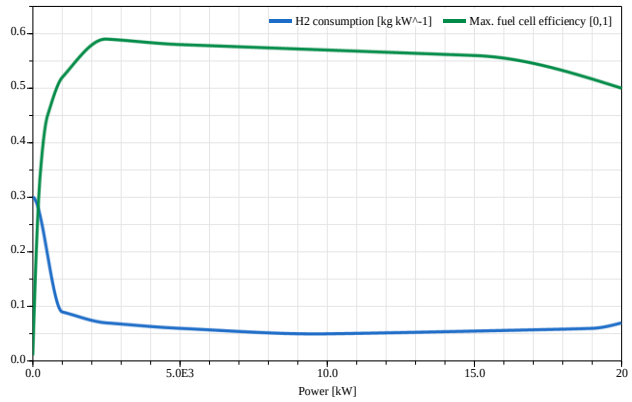

Figure 6: Efficiency and hydrogen consumption map of the fuel cell based on [25]

F. *Vehicle Motion Controller*

The longitudinal velocity control relies on a linear PI controller [26]. The lateral controller uses a model inversion technique to follow the reference curvature (ρ^*) generated by the mission planner. It makes use of a simplified single-track model [27]

$$\begin{aligned} \dot{x}_{STM} &= A(v^*)x_{STM} + B(v^*)\delta^* \\ &\quad + E(v^*)M_{z,TV} \\ \dot{\beta}^* &= v^*\rho^* - r^* \end{aligned} \tag{16}$$

where $x_{STM} = [\beta^*, r^*]^T$ is vector with the reference side-slip angle and yaw rate; $A(v^*)$ and $E(v^*)$ are matrices that depend on the vehicle velocity; $M_{z,TV}$ is the torque vectoring generated by the in-wheel motors:

$$M_{z,TV} \approx \frac{c}{2r}(\tau_R^* - \tau_L^*) = \frac{c\tau^*}{2r}(2\alpha_{TV} - 1) \tag{17}$$

where r is the wheel radius and c the vehicle's track width. Assuming slow variations in vehicle curvature we can obtain

$$\begin{aligned} 0 &\approx A(v^*)x_{STM} + B(v^*)\delta^* + E(v^*)M_{z,TV} \\ 0 &\approx v^*\rho^* - [0,1]x_{STM} \end{aligned} \tag{18}$$

which represents a system of three linear equations with three unknowns $(\delta^*, x_{STM}) = (\delta^*, \beta^*, r^*)$. The steering angle applied to the vehicle is computed from the solution of these equations:

$$\delta^* = f_\delta(v^*, M_{z,TV}, \rho^*) \tag{19}$$

This represents a feedforward control law, which allows the vehicle to follow the reference curvature (ρ^*) when the model uncertainty is reduced.

IV. Energy Management Algorithm

This section provides a brief overview of the requirements for the EMA that the competitors will need to develop, as well the scoring and ranking assessment of the competition.

A. *Input/Output Interfaces*

The EMA will have access to the following vehicle states

$$x = \left[v, a, SoC_b, T_b, SoC_{FC}, \widehat{W}\right] \in X_{EMA} \tag{20}$$

which contain the current velocities v, accelerations a, state of charge SoC_b and temperature of the battery T_b, and the state of charge of the fuel cell SoC_{FC}. The variable $\widehat{W}$ is a vector with a short preview information about the reference velocity and track curvature

$$\widehat{W} = \left(v^*(t + k\Delta t), \rho^*(t + k\Delta t)\right)_{k=0}^{N_{pre}} \tag{21}$$

where Δt is the sample time and N_{pre} are the samples of the preview window. We denote X_{EMA} as the set of all possible combinations of states that the EMA might receive.

The EMA generates four output control signals, see Section II.C,

$$u = [\alpha_{FC}, \alpha_{AD}, \alpha_{TV}, \alpha_v] \in U = [0,1]^4 \tag{22}$$

where U represents the set of allowed control actions.

B. *Safety Constraints*

The competitors will provide a control policy π for the energy management that maps the states into the control actions

$$\pi(x): X_{EMA} \to U. \tag{23}$$

This policy will need to fulfill two type of safety constraints. The first are state of charge constraints of the energy storage devices:

$$\begin{aligned} X_{safe,SOC} = \{&x_{EMA} \in X_{EMA} \\ &SoC_{b,min} \le SOC_b \le SoC_{b,max} \\ &SoC_{FC,min} \le SOC_{FC} \\ &\le SoC_{FC,max}\} \end{aligned} \tag{24}$$

where $SoC_{b,min}, SoC_{FC,min}$ represent the minimum SoC levels for the energy storage devices, and $SoC_{b,max}, SoC_{FC,max}$ their maximum values. The second set of constraints is the battery temperature

$$X_{safe,T} = \{x_{EMA} \in X_{EMA}:\ T_{bat} \le T_{bat,max}\} \tag{25}$$

This set of constraints can be temporarily violated; however, these violation increases the risk of failure of this component (e.g. thermal runaway [28]) and are penalized in the EMA performance score.

C. *Performance Metrics*

The EMA will be evaluated using the following performance metrics (see also Table 2).

- J_E: Total energy consumption of the vehicle. It is computed by integrating the power delivered by the battery (p_{bat}) and the fuel cell (p_{FC}).
- J_{SoC}: timespan that SoC constraints $X_{safe,SOC}$ are violated.

- J_{TC}: timespan that the thermal constraints $X_{safe,T}$ are violated.
- J_{deg}: battery capacity that is lost during the vehicle mission due to battery cycle aging.
- J_v : derating metric that captures ability of the vehicle to track the velocity profile defined by the mission planning.

Table 2: Summary of performance metrics

Metric	Formula
J_E	$\int_0^{t_{end}} p_{bat}(t) + p_{FC}(t)dt$
J_{SoC}	$\int \mathbb{1}_{\{x(t)\notin X_{safe,SOC}\}}dt$
J_{TC}	$\int \mathbb{1}_{\{x(t)\notin X_{safe,T}\}}dt$
J_{deg}	$\frac{\mathrm{d}\Delta C_{cell}(i_{avg},T_{avg})}{dN}$
J_v	$\int (1-\alpha_v(t))dt$

$\mathbb{1}_{\{cond\}}$ is a function that returns 1 if $cond = 1$, and zero otherwise

Note that the value of these performance metrics will be dependent on the EMA provided by the algorithm $\pi(x)$ and the mission profile:

$$W = \left(v^*(t_k), \rho^*(t_k)\right)_{k=1}^{N} \tag{26}$$

D. EMA Baseline Policy

Consider the following baseline EMA policy

$$\tilde{\pi}(x) = [\tilde{\alpha}_{FC}(x), \tilde{\alpha}_{AD}(x)\ \tilde{\alpha}_{TV}(x), \tilde{\alpha}_v(x)] \tag{27}$$

$$\tilde{\alpha}_{FC}(x) = \begin{cases} k_{FC} & \text{if } x(t) \in X_{safe,SOC} \\ 0 & \text{otherwise} \end{cases} \tag{28}$$

$$\tilde{\alpha}_{AD}(x) = 1/2 \tag{29}$$

$$\tilde{\alpha}_{TV}(x) = k_{TV}\rho^*(v^*)^2 \tag{30}$$

$$\tilde{\alpha}_v(x) = \begin{cases} 1 & \text{if } x(t) \in X_{safe,SOC} \\ 0 & \text{otherwise} \end{cases} \tag{31}$$

This policy enforces

- constant usage of the fuel cell (with ratio k_{FC}) if safety constraints are fulfilled (eq. (28)); it disables the fuel cell and vehicle usage ($\alpha_v = 0$) whenever violation of SoC constraints occur (eq. (31))
- constant front-rear torque distribution ratio (eq. (29))
- a torque allocation policy proportional to the expected lateral acceleration of the vehicle ($\rho^*(v^*)^2$); where k_{TV} is a constant; ii); iii) (eq. (30))

This baseline policy generates baseline metrics, which are denoted as:

$$\tilde{J}_E, \tilde{J}_{SoC}, \tilde{J}_{TC}, \tilde{J}_{Deg}, \tilde{J}_v \tag{32}$$

E. Evaluation and Ranking

The score of the EMA over a given mission profile is computed as a weighted summation of the performance metrics, normalized with respect to the EMA baseline policy ($\tilde{\pi}$). Mathematically, this means:

$$J = k_E\frac{J_E}{\tilde{J}_E} + k_{SoC}\frac{J_{SoC}}{\tilde{J}_{SoC}} + k_{TC}\frac{J_{TC}}{\tilde{J}_{TC}} + k_{Deg}\frac{J_{Deg}}{\tilde{J}_{Deg}} + k_v\frac{J_v}{\tilde{J}_v} \tag{33}$$

where $k_E, k_{TC}, k_{Deg}, k_v$ are known weights (defined by the organizers) and $J_E, J_{SoC}, J_{TC}, J_{Deg}, J_v$ are the performance metrics obtained with the EMA provided by the competitor, $\pi(x)$. Note that the overall score of the EMA depends not only on the policy $\pi(x)$, but also on the mission profile W, i.e.,

$$J(\pi, W) \tag{34}$$

The evaluation will consider a bank of mission profiles. $W_1, W_2, \dots, W_M$, which contain typical operating conditions for the vehicle. Each profile can be selected with probability

$$p(W_j) = p_j, \quad j = 1, \dots, M \tag{35}$$

Some driving cycles (but not all) will be provided to the competitors; the driving cycle probability (p_j) is also unknown to the competitors. The performance of an EMA will be performed based on the average cost over all mission profiles:

$$\mathbb{E}\{J(\pi, W)\} = \sum_{j=1}^{M} p(W_j)J(\pi, W_j) \tag{36}$$

where $\mathbb{E}\{.\}$ is the expected value operator (over W). The final EMA ranking will be performed as follows. We will collect all the energy management algorithms provided by the competitors, $\pi_1, \dots, \pi_L$, where L is the number of received submissions. The competitor that provides the lowest average cost will be the winner, i.e.:

$$L_{winner} = \arg \min_{l\in\{1,\dots,L\}} \mathbb{E}\{J(\pi_l, W)\} \tag{37}$$

V. Summary and Outlook

This article presented the concept, modeling and setup for the IEEE Motor Vehicle Challenge 2023, which differs highly from the last years' challenges. It relies on a multi-domain modeling approach using Modelica and FMI technology as well as an integrated vehicle control with trajectory following. The focus of the challenge is on the design of complex vehicle and control architecture, as described in Chapter II, giving the competitors normalized tuner input variables for their EMA that directly affect the vehicle's powertrain and therefore the energy consumption. Moreover, we described in Chapter III our modelling approaches, which are on a detail level of functional models in combination with characteristic tables and fundamental physical equations of the particular domain as well as the vehicle motion controller which tracks the trajectories (spatial and velocity profile) by means of Modelica's powerful technology of inverse models. Finally, Chapter IV described all variables available to the competitors, constraints we impose on the criteria and performance metrics for the assessment of their EMA algorithm. Moreover, a reference implementation of a

baseline EMA is employed for which more information is provided in the Appendix Chapter VI. The point metric will help the competitors to tune their algorithm to achieve a best possible result. Future points of interest in research are the development of more complex vehicle components and architectures which are tuned and validated with real world experiments.

Author Contributions: Conceptualization, J.B., R.C., and J.T.; methodology, J.B., R.C., and J.T. Modelica vehicle model and components, J.B., and J.T.; controller and trajectories, R.C., and J.B.; EMA assessment and baseline algorithm: R.C. and J.B., library management and testing J.T.; writing—original draft preparation, R.C., J.B., and J.T.; All authors have read and agreed to the published version of the manuscript. *Acknowledgement:* Lenzo Basilio testing of challenge data and models. *Funding*: internal institutional funding of the DLR granted by the Helmholtz Association of German Research Centres HGF.

VI. Appendix

For the final submission we plan to give a reference implementation of the described EMA baseline policy in Chapter IV.D. This will be hosted on a Git repository (https://github.com/dlr-vsdc) with the baseline EMA algorithm and it's results to help the competitors to assess their developments and to get an easier start by means of this reference implementation. Furthermore, all used parameters from the vehicle and its components will be listed to support the competitor's controller synthesis process. We shortly describe the planned trajectories for testing & evaluating the EMA algorithms. These might be extended in the final submission:

- Example 1: highway driving with $\rho^* \approx 0$ almost everywhere.
- Example 2: use DLR's driving cycle from Techlab to train station

Repository links to publicly available libraries used here:
https://github.com/modelica/ModelicaStandardLibrary
https://github.com/modelica/VehicleInterfaces
https://github.com/dzimmer/PlanarMechanics

VII. References

[1] E. Amaya, H. Chiacchiarini, C. De Angelo und M. Asensio, „The Energy Management Strategy of FC/Battery Vehicles Winner of the 2017 IEEE VTS Motor Vehicles Challenge," in *The Energy Management Strategy of FC/Battery Vehicles Winner of the 2017 IEEE VTS Motor Vehicles Challenge*, 2017.

[2] A. Ferrara und H. C., „Rule-Based Energy Management Strategy of Fuel Cell/Ultracapacitor/Battery Vehicles: winner of the IEEE VTS Motor Vehicles Challenge 2020,," in *2020 IEEE Vehicle Power and Propulsion Conference*, 2020.

[3] B. Nguyen; J. P. F. Trovão; S. Jemei; L. Boulon; A. Bouscayrol, „IEEE VTS Motor Vehicles Challenge 2021 - Energy Management of A Dual-Motor All-Wheel Drive Electric Vehicle," in *IEEE Vehicle Power and Propulsion Conference (VPPC)*, 2021.

[4] C. Depature, S. Pagerit, L. Boulon, S. Jemei, A. Jemei und A. Bouscayrol, „IEEE VTS Motor Vehicles Challenge 2018 - Energy Management of a Range Extender Electric Vehicle," in *IEEE Vehicle Power and Propulsion Conference (VPPC)*, 2017.

[5] H. Pereira, R. de Castro, R. E. Araújo, „How to Win the 2021 IEEE VTS Motor Vehicles Challenge With a Pragmatic Energy Management Strategy," in *IEEE Vehicle Power and Propulsion Conference (VPPC)*, 2021.

[6] T. Vo-Duy, J. P. F. Trovão, S. Jemeï, L. Boulon, M. C. Ta und A. Bouscayrol, „IEEE VTS Motor Vehicles Challenge 2022 - Sizing and Energy Management of Hybrid dual-Energy Storage System for a Commercial Electric Vehicle," in *2021 IEEE Vehicle Power and Propulsion Conference (VPPC)*, 2021.

[7] J. Solano, S Jemei, L Boulon, L Silva, D Hissel, M-C Pera, „IEEE VTS motor vehicles challenge 2020-energy management of a fuel cell/ultracapacitor/lead-acid battery hybrid electric vehicle," in *IEEE Vehicle Power and Propulsion Conference (*, 2019.

[8] W. Lhomme; T. Letrouve; L. Boulon; S. Jemei; A. Bouscayrol; F. Chauvet; F. Tournez, „IEEE VTS Motor Vehicles Challenge 2019 - Energy Management of a Dual-Mode Locomotive," in *IEEE Vehicle Power and Propulsion Conference (VPPC)*, 2018.

[9] R. de Castro, M. Tanelli, R. E. Araújo und S. M. Savaresi, „Design of safety-oriented control allocation strategies for overactuated electric vehicles," *Vehicle System Dynamics*, Bd. 52, pp. 1017-1046, 2014.

[10] J. Torinsson, M. Jonasson, D. Yang und B. Jacobson, „Energy reduction by power loss minimisation through wheel torque allocation in electric vehicles: a simulation-based approach," *Vehicle System Dynamics*, Bd. 60, pp. 1488-1511, 2022.

[11] B. Lenzo, „Torque Vectoring Control for Enhancing Vehicle Safety and Energy Efficiency," in *Vehicle Dynamics: Fundamentals and Ultimate Trends*, B. Lenzo, Hrsg., Cham, Springer International Publishing, 2022, p. 193–233.

[12] C. Chatzikomis, A. Sorniotti, P. Gruber, M. Zanchetta, D. Willans und B. Balcombe, „Comparison of Path Tracking and Torque-Vectoring Controllers for Autonomous Electric Vehicles," *IEEE Transactions on Intelligent Vehicles*, Bd. 3, pp. 559-570, 2018.

[13] R. de Castro und J. Brembeck, „Lyapunov-based fault tolerant control allocation," *Vehicle System Dynamics*, Bd. 0, pp. 1-26, 2021.

[14] J. Brembeck, L. M. Ho, A. Schaub, C. Satzger, J. Tobolar, J. Bals und G. Hirzinger, „ROMO - The Robotic Electric Vehicle," in *22nd IAVSD International Symposium on Dynamics of Vehicle on Roads and Tracks*, Manchester Metropolitan University, 2011.

[15] J. Brembeck und P. Ritzer, „Energy optimal control of an over actuated Robotic Electric Vehicle using enhanced control allocation approaches," in *Proceedings of the 2012 IEEE Intelligent Vehicles Symposium*, Alcala de Henares, Spain, 2012.

[16] J. Brembeck, „Model Based Energy Management and State Estimation for the Robotic Electric Vehicle ROboMObil," Ph.D. dissertation, Technical University of Munich, Munich, Germany, 2018.

[17] Modelica Association, „Modelica," 2022. [Online]. Available: http://www.modelica.org. [Zugriff am 05 01 2022].

[18] R. de Castro, T. Bünte und J. Brembeck, „Design and Validation of the Second Generation of the Robomobil's Vehicle Dynamics Controller," in *24th Symposium of the International Association for Vehicle System Dynamics*, Graz, Austria, 2016.

[19] J. Ultsch, J. Mirwald, J. Brembeck und R. de Castro, „Reinforcement Learning-based Path Following Control for a Vehicle with Variable Delay in the Drivetrain," in *31st IEEE Intelligent Vehicles Symposium*, 2020.

[20] T. Bünte, L. M. Ho, C. Satzger und J. Brembeck, „Central Vehicle Dynamics Control of the Robotic Research Platform ROboMObil," *ATZelektronik worldwide*, June 2014.

[21] D. Zimmer und M. Otter, „Real-time models for wheels and tyres in an object-oriented modelling," *Vehicle System Dynamics*, 2009.

[22] R. de Castro, H. Pereira, R. E. Araújo, J. V. Barreras und H. C. Pangborn, „qTSL: A Multilayer Control Framework for Managing Capacity, Temperature, Stress, and Losses in Hybrid Balancing Systems," *IEEE Transactions on Control Systems Technology*, Bd. 30, pp. 1228-1243, 2022.

[23] D. Feroldi, M. Serra und J. Riera, „Energy Management Strategies based on efficiency map for Fuel Cell Hybrid Vehicles,“ *Journal of Power Sources,* Bd. 190, pp. 387-401, 2009.

[24] K. J. Åström und R. M. Murray, Feedback Systems: An Introduction for Scientists and Engineers, Second Edition, Princeton University Press, 2021.

[25] J. Ackermann, P. Blue, T. Bünte, L. Guvenc, D. Kaesbauer, M. Kordt, M. Muhler und D. Odenthal, Robust Control: The Parameter Space Approach, 2002.

[26] X. Feng, D. Ren, X. He und M. Ouyang, „Mitigating Thermal Runaway of Lithium-Ion Batteries,“ *Joule,* Bd. 4, pp. 743-770, 2020.

[27] J. Brembeck, „A Physical Model-Based Observer Framework for Nonlinear Constrained State Estimation Applied to Battery State Estimation,“ *Sensors,* Bd. 19, Nr. 20, p. 4402, 2019.